1 **MiR-409-3p targets a MAP4K3-ZEB1-PLGF signaling axis and controls brown adipose**

2 **tissue angiogenesis and insulin resistance**

3

4 **Authors**: Dakota Becker-Greene[1], Hao Li[1], Daniel Perez-Cremades[1,2], Winona Wu[1], Furkan
5 Bestepe[3], Denizhan Ozdemir[1,4], Ceren Aydogan[1,5] Dennis P. Orgil[6], Mark W. Feinberg[1†], and
6 Basak Icli[1,3†].
7

8 †Corresponding author.

9

10 **Author Affiliations**:

11 [1] Cardiovascular Division, Department of Medicine, Brigham & Women's Hospital, Harvard
12 Medical School, Boston, MA, 02115.

13 [2] Department of Physiology, University of Valencia and INCLIVA Biomedical Research Institute,
14 Valencia, Spain.

15 [3] Molecular Cardiology Research Institute, Tufts University Medical School, Boston, MA, 02111.

16 [4] Department of Medical Biology, Hacettepe University, Ankara, Turkey.

17 [5] Cerrahpasa Faculty of Medicine, Istanbul, Turkey.

18 [6] Division of Plastic Surgery, Department of Surgery, Brigham and Women's Hospital, Harvard
19 Medical School, Boston, MA 02115.

20

21

22 *** Correspondence:**

23 Basak Icli, MS, PhD, Molecular Cardiology Research Institute, Tufts University Medical School,
24 800 Washington St, Boston, Massachusetts, USA, 02111. E-mail: bicli@tuftsmedicalcenter.org,
25 Tel: (617) 636-9163

26 Correspondence can also be directed to: Mark W. Feinberg, MD, Department of Medicine,
27 Cardiovascular Division, Brigham and Women's Hospital, Harvard Medical School, Louis
28 Pasteur Avenue 77, 02115, Boston, Massachusetts, USA, 02115. E-mail:
29 mfeinberg@bwh.harvard.edu, Tel: (617) 525-4381

30

31 Short title: MiR-409-3p regulates MAP4K3/ZEB1/PLGF**,** angiogenesis and insulin resistance
32

33 **Keywords:** Angiogenesis, Brown Adipose Tissue, Fat Browning, Non-coding RNAs, Obesity
34 **Manuscript Word Count:** 4408
35 **Figures:** 7 main, 8 supplemental **Tables:** 2 supplemental
36 **References:** 63

Abstract

Endothelial cells (ECs) within the microvasculature of brown adipose tissue (BAT) are important in regulating the plasticity of adipocytes in response to increased metabolic demand by modulating the angiogenic response. However, the mechanism of EC-adipocyte crosstalk during this process is not completely understood. We used RNA sequencing to profile microRNAs derived from BAT ECs of obese mice and identified an anti-angiogenic microRNA, miR-409-3p. MiR-409-3p overexpression inhibited EC angiogenic properties; whereas, its inhibition had the opposite effects. Mechanistic studies revealed that miR-409-3p targets ZEB1 and MAP4K3. Knockdown of ZEB1/MAP4K3 phenocopied the angiogenic effects of miR-409-3p. Adipocytes co-cultured with conditioned media from ECs deficient in miR-409-3p showed increased expression of BAT markers, UCP1, and CIDEA. We identified a pro-angiogenic growth factor, placental growth factor (PLGF), released from ECs in response to miR-409-3p inhibition. Deficiency of ZEB1 or MAP4K3 blocked the release of PLGF from ECs and PLGF stimulation of 3T3-L1 adipocytes increased UCP1 expression in a miR-409-3p dependent manner. MiR-409-3p neutralization improved BAT angiogenesis, glucose and insulin tolerance, and energy expenditure in mice with diet-induced obesity. These findings establish miR-409-3p as a critical regulator of EC-BAT crosstalk by modulating a ZEB1-MAP4K3-PLGF signaling axis, providing new insights for therapeutic intervention in obesity.

64 **Non-standard Abbreviations and Acronyms**

65	T2D	Type 2 Diabetes Mellitus
66	EC	Endothelial cell
67	HUVECs	human umbilical vein ECs
68	HUAECs	human umbilical arterial ECs
69	miRNA	microRNA
70	NS	nonspecific
71	RT-PCR	Real-time polymerase chain reaction
72	siRNA	small interfering RNA
73	3'-UTR	3'-untranslated region
74	ZEB1	Zinc Finger E-Box Binding Homeobox
75	MAP4K3	Mitogen-activated protein kinase kinase kinase kinase 3
76	PLGF	Placental Growth Factor
77	FLT1	Fms-like Tyrosine Kinase-1
78	BAT	Brown Adipose Tissue
79	WAT	White Adipose Tissue
80	DIO	Diet Induced Obesity

81

82 **Introduction**

83 Obesity is primarily caused by an imbalance between energy intake and expenditure, leading to
84 increased body weight and overall adipose tissue enlargement [1]. This increase in obesity
85 parallels type 2 diabetes (T2D) with approximately 1 in 10 adults diagnosed with T2D in the US
86 accompanied by a marked increase in healthcare expenditures [2-4].

87

88 There are two main adipose tissue depots: white adipose tissue (WAT), which primarily stores
89 energy, and brown adipose tissue (BAT), which consumes energy through thermogenesis [5].
90 The presence of active BAT in human adults opened a new avenue of inquiry for the
91 development of obesity and insulin resistance in adults [6-8]. Both WAT and BAT are highly
92 vascularized. Studies in mice show that visceral adipose tissue can double in size after the first
93 week of high-fat diet (HFD), but will undergo significant reduction following 24 hours of fasting
94 [9]. This plasticity is orchestrated by endothelial cells (ECs), fibroblasts, and immune cell
95 subsets, that release various cytokines, growth factors, and adipokines, leading to angiogenesis
96 and remodeling of the extracellular matrix [10].

97

98 Impaired angiogenesis in adipose tissue is linked to diet-induced obesity (DIO) and insulin
99 resistance [11]. A corresponding maladaptive consequence is the whitening of BAT that
100 attenuates the thermogenic response, alters glucose metabolism, and decreases BAT mass in
101 obese subjects [12]. Furthermore, targeted inhibition of neovascularization in advanced adipose
102 tissue halts obesity progression; whereas, enhancing neovascularization in developmentally
103 early-stage adipose tissue leads to healthy fat pads that confer favorable metabolic properties
104 [13]. This is consistent with the absence of small vessel formation during diet-induced obesity
105 (DIO) when migration, proliferation, and adhesion of ECs become impaired [14, 15].

106

107 There is a delicate balance between pro- and anti-angiogenic factors that regulate
108 angiogenesis. They target ECs to alter migration and proliferation, and are secreted by adipose

109 tissue, suggesting an autoregulatory function[16-18]. Of these factors, vascular endothelial
110 growth factor-A (VEGF-A), a known contributor to vasculogenesis, angiogenesis, and tissue
111 remodeling, facilitates pro-angiogenic activity. Reduced VEGF-A activity has been observed in
112 the subcutaneous adipose tissue of obese subjects [10, 18-20]. Transplantation of VEGF-A
113 overexpression in adipose tissue improved systemic metabolism through increased
114 angiogenesis and beiging of subcutaneous (s)WAT, suggesting a protective effect[21]. In
115 addition, BAT-specific expression of VEGF-A in obese mice was associated with increased
116 vascularity, improved BAT function and insulin sensitivity [22]. Furthermore, transplantation of
117 BAT in mice with DIO demonstrated improved overall metabolism [23]. However, other studies
118 have shown that VEGF-A is increased in obese mice, demonstrating the complexity of
119 angiogenesis in obesity and the necessity for a better understanding of endothelial-adipocyte
120 interactions [24, 25].
121
122 Placental growth factor (PLGF) is a member of the VEGF family. Unlike VEGF, which binds to
123 both VEGF receptor (VEGFR)-1 (also named as fms-like tyrosine kinase-1 or FLT1) and
124 VEGFR-2, PLGF only binds to FLT1 [26]. Through the activation of FLT1, PLGF induces
125 signaling pathways different from those induced by VEGF via inducing the phosphorylation of
126 distinct tyrosine residues of FLT1 [27]. Many cell types including ECs produce PLGF under
127 pathological conditions. In the vascular system, PLGF was shown to induce angiogenesis by
128 promoting proliferation and migration of endothelial cells [28]. In adipose tissue, PLGF inhibition
129 reduced formation of de novo fat pad without affecting adipose tissue development [29] thereby
130 suggesting a role in early stages of adipogenesis. On the other hand, PLGF deficiency reduced
131 the fraction of brown adipocytes while stimulating white adipocyte hypertrophy in mice fed a
132 high-fat diet [30].
133
134 MicroRNAs (miRNAs) are evolutionarily conserved small noncoding RNAs that inhibit gene
135 expression at the post-transcriptional level, thereby serving as physiological “fine-tuners” with

136 therapeutic potential [31, 32]. Distinct miRNA expression signatures have been observed in
137 obese mice and humans when compared to their lean counterparts [33-35]. For example,
138 expression of the anti-inflammatory miR-181b was reduced in adipose tissue ECs and delivery
139 of miR-181b to the microvasculature significantly improved insulin resistance in mice [13].
140 Knockdown of the Let-7 family of miRNAs improved glucose tolerance in DIO mice [36, 37].
141 Similarly, miR-143 and miR-145 were upregulated in the liver of obese mice, while mice
142 deficient in the miR-143-145 cluster were protected from obesity-induced insulin resistance [38].
143 Furthermore, silencing of miR-103 and miR-107 led to improved glucose homeostasis, but were
144 overexpressed at baseline in obese mice [39]. These miRNAs illustrate their potential to impact,
145 either positively or negatively, the development and progression of insulin resistance. However,
146 the role of miRNAs in the regulation of the microvasculature of BAT remains poorly understood.
147
148 In this report, we identified that miR-409-3p plays a key regulatory role in EC-BAT crosstalk by
149 modulating a MAP4K3 and ZEB1–placental growth factor (PLGF) signaling axis, impacting
150 angiogenesis, obesity, and insulin resistance. Our findings reveal that targeting miR-409-3p may
151 represent a new therapeutic approach in DIO by accelerating browning of adipose tissues and
152 improving energy metabolism.
153
154 **Methods**
155 ***Cell Culture and Transfection***
156 Human umbilical vein endothelial cells (HUVECs) (Lonza) cultured in EGM®-2 (Lonza,) were
157 transfected using Lipofectamine™ 2000 (Invitrogen). For reporter studies, HUVECs were
158 transfected with 400 ng of the indicated reporter and either 30nM miR-409-3p mimic (Thermo
159 Scientific, 4464066) or 100nM miR-409-3p inhibitor (Thermo Scientific, 4464084). Gene
160 knockdown experiments were conducted with control (Dharmacon, D-001810-10) or target of
161 interest siRNA specified for each experiment.
162

163 ***Luciferase Reporter Assay***

164 HUVECs were transfected with 400 ng of MAP4K3 (HmiT021033, Genecopoeia) or ZEB1 3'-
165 UTR (HmiT067039, Genecopoeia) per well followed by 30nM miR-409-3p mimic, 200nM miR-
166 409-3p inhibitor, or equivalent non-specific controls 24 hrs later. Luciferase Reporter Assay
167 (Promega, E1500) was used and normalized to the total protein in each well (Thermo Scientific,
168 23227).

169 ***Differentiation of 3T3-L1 Preadipocytes into Mature Brown-like Adipocytes***

170 3T3-L1 cells (ATCC) were cultured in maintenance media (MM), induced using induction media
171 (IM) and the time point was marked as Day 1 (D1). On D3, media was switched to a
172 differentiation media (DM) and EC conditioned media co-culture started at a 1:1 ratio. Both the
173 differentiation and the EC conditioned media were replenished every 2 days. On D7-D8, cells
174 were harvested. MM was composed of DMEM with F12 and HEPES supplemented with 10%
175 Fetal Calf Serum (FCS) (GeminiBio, 100-504), and 1% P/S. IM was prepared with MM
176 supplemented with 10 uM/L human insulin, 0.5 mmol/L IBMX, 0.25 umol/L dexamethasone, and
177 1 nM T_3 [40]. DM was prepared with MM supplemented with 10 uM/L human insulin, 1 nM T_3, 1
178 uM rosiglitazone [41, 42].

179 ***Gene Expression Analysis***

180 RNA was harvested in TRIzol® reagent. Reverse transcription was performed using miScript
181 Reverse Transcription Kit (Qiagen, 218061). QuantiTect SYBR Green RT-PCR Kit (Qiagen,
182 204243) or miScript SYBR Green PCR Kit (Qiagen, 218073) were used for RT-qPCR studies
183 (AriaMx, Agilent Technologies) using gene-specific primers (Supplemental Table 1) normalized
184 to HPRT or GAPDH. Mature miRNA sequences were amplified with Hs_miR-409-3p_1 (Qiagen,
185 MS00006895) and normalized to Hs_RN5S1_11 (Qiagen, MS00007574). Fold changes were
186 calculated by the ΔΔCt method.

187 ***Western Blotting***

188 Total protein was isolated in RIPA buffer (Boston BioProducts, BP-115) with 1X Halt™ protease
189 inhibitor (Thermo Scientific, 1861261) and quantified by BCA (Thermo Scientific, 23225).

190 Lysates were separated using 5-15% Mini-PROTEAN TGX Precast Gels (Bio-Rad) and
191 subjected to Western blotting using Abcam antibodies against ZEB1 (ab124512), MAP4K3
192 (ab173308), UCP1 (ab155117), CIDEA (ab8408), CST antibodies against α-Tubulin (2144), β-
193 actin (4970), goat anti-rabbit (7074) or anti-mouse antibodies (7076). ECL assay was performed
194 (RPN2132; GE Healthcare) and quantification was conducted (Image-J).

195 ***Tube-like network formation on Matrigel***

196 Matrigel (BD Bioscience) assay was performed as we previously described [43, 44].

197 ***Chemotaxis Assays***

198 Migration assay was performed using ChemTX multiwell system (Neuro probe). The number of
199 cells migrating to the lower chamber (EC growth media with 50ng/ml VEGF or bFGF as
200 indicated) was counted after 6-8 hours [43].

201 ***BrdU Assay***

202 BrdU ELISA assay (Roche, 116472290001) was performed, as we previously described [44].

203 ***MiRNP immunoprecipitation (MiRNP-IP)***

204 MiRNP-IP was performed as we previously described [45].

205 ***Scratch Assay***

206 Scratch assay was performed as we previously described [44] and cells were imaged using
207 Eclipse TE2000-U inverted microscope (Nikon).

208 ***Human Adipose Organoids***

209 Full-thickness circular (3-mm) human adipocyte organoids were taken from subcutaneous white
210 adipose tissue post abdominal surgery and cultured in maintenance media (MM) referred to as
211 day 0 (D0). On D1, media was changed to induction media (IM). On D3 and D5, the media was
212 replaced with a 1:1 ratio of differentiation media (DM including rosiglitazone to induce browning
213 [46, 47]: EC conditioned media (transfected 72 hours prior with indicated NS controls or miR-
214 409 mimic or inhibitors). Organoids were harvested on D7 using aforementioned methods. MM
215 was composed of Dulbecco’s Modified Eagle’s Medium (DMEM) with 4.5 g/L glucose and with
216 L-glutamine (Lonza) supplemented with 10% FBS and 1% P/S. IM was composed of MM with

217 0.5 mmol/L IBMX, 0.25 umol/L dexamethasone, 1 nM T_3 and 10 uM/L human insulin. DM was
218 composed of MM with 10 uM/L human insulin, 1 nM T_3, and 1 uM rosiglitazone. The viability of
219 cultured explants was validated by histologic evaluation performed on Days 0, 3, 5 and 7 for
220 adipose density and structure by H&E and perilipin 1 (PLIN1) stainings (Data not shown).
221 Angiogenesis was analyzed by CD31 staining (28364; Abcam), DAPI (H21492; Invitrogen) for
222 nuclear staining and Alexa 647 conjugated donkey anti-rabbit antibody for secondary antibody
223 (711-605-152; Jackson ImmunoResearch). Relative CD31 expression was measured in the
224 entire cross-section of the human organoid and quantified using Image J.

225 ***Metabolic Studies***

226 Mice fasted for 12 hours received intra-peritoneal (i.p.) injection of D-glucose (1U/kg, Sigma,
227 G8270) for glucose tolerance test (GTT). For insulin tolerance test (ITT), mice were fasted for 6
228 hours and i.p. injected with 0.75U/kg insulin. Blood glucose measurements were taken prior to
229 injections and at 15, 30, 45, 60, 90, and 120 minutes after glucose or insulin injection
230 (OneTouch, LifeScan). Whole-body energy expenditure was measured at ambient temperature
231 (~22°C) using Columbus Comprehensive Lab Animal Monitoring System.

232 ***Histological and Immunohistological Examinations***

233 Tissues were fixed with 10% formalin solution, embedded in parafin wax, cut into 10um
234 sections, and then deparafinized. Images were acquired on an upright Carl Zeiss LSM 510
235 confocal microscope. Data was analyzed in a blinded fashion using the Volocity Software
236 (Quorum Technologies). For Oil red O staining, cells were fixed with 10% formaldehyde for
237 15 min at room temperature and stained using the Oil red O working solutions (5 g/l in
238 isopropanol) and 4 ml ddH_2O for 30 min. After staining, the cells were washed with 60%
239 isopropanol and images were acquired on an Eclipse TE2000-U inverted microscope (Nikon).

240 ***Animal Care and Use***

241 Animal studies were approved by the Institutional Animal Care and Use Committee. For DIO,
242 male, 4 weeks old, C57BL/6 mice (Charles River) were placed on high-fat diet (HFD) containing

243 60 kcal% fat (Research Diets, D12492), received weekly tail-vein injections of scrambled control

244 LNA-anti-miR or LNA-anti-miR-409 (10 mg/kg ,Exiqon) for 11 weeks.

245 ***Statistical Analysis***

246 Data are presented as mean ± SEM. Sample sizes for mouse and human organoid experiments

247 were chosen based upon pilot or similar well-characterized studies in the literature. There were

248 no inclusion or exclusion criteria used. Data were subjected to unpaired two-sided Student's t-

249 test or one-way ANOVA with Bonferroni correction for multiple comparisons, and $P<0.05$ was

250 considered statistically significant.

251 ***Data and Resource Availability***

252 The data generated from this study and the associated resources are available from the

253 corresponding authors upon reasonable request.

254

255 **Results**

256 To identify miRNAs in the microvasculature of brown fat that might impact metabolic dysfunction

257 in obesity, ECs were isolated from C57BL/6 mice after 8 weeks of chow or HFD and subjected

258 to miRNA-seq profiling (fold-change >2; FDR p<.05). MiR-409-3p was identified as a top

259 significantly regulated miRNA that increased with HFD (Fig. 1B and Supplemental Fig. 1A).

260 Expression of miR-409-3p was highest in multiple EC cell types, including HUVECs and human

261 umbilical artery endothelial cells (HUAECs) compared to non-EC cell lines, such as human pre-

262 adipocytes, human adipocytes, mouse spleen and bone marrow monocytes, and human

263 fibroblasts (Fig. 1C). Furthermore, separation of ECs from non-ECs from the brown fat of mice

264 fed HFD for 8 weeks demonstrated a 2-fold increased expression of miR-409 in the EC fraction

265 (Supplemental Fig. 1B). Overall, this data demonstrates that miR-409-3p is highly expressed in

266 mouse brown fat ECs under diet induced obesity conditions.

267

268 To examine the functional role of miR-409-3p, *in vitro* gain- and loss-of-function studies were

269 performed. Compared to non-specific controls (NS_m), overexpression of miR-409-3p in HUVECs

270 using miR-409-3p mimics (miR-409_m) demonstrated a 35% reduction in proliferation as
271 assessed by BrdU assay (Fig. 1D) and a 50% diminished wound closure rate using EC scratch
272 assays (Fig. 2C). HUVECs transfected with miR-409_m showed a 50% reduction in cumulative
273 sprout length (Fig. 2E) and 29% reduction in the number of tubes as quantified by network tube
274 formation in Matrigel (Fig. 2G). In accordance with these findings, miR-409-3p reduced the
275 number of cells per well by 37% when assessed by transwell migration (Fig. 2A). In contrast,
276 when miR-409-3p was blocked using miR-409-3p inhibitors (miR-409_i), it triggered a 1.5-fold
277 increase in proliferation as assessed by BrdU assay (Fig. 1E) and a 3-fold increase in wound
278 closure rate by scratch assay compared to non-specific controls (NS_i) (Fig. 2D). In line with
279 these findings, miR-409-3p inhibition also increased EC sprout length by 1.4-fold (Fig. 2F),
280 network tube formation by 2.75-fold in Matrigel (Fig. 2H), and the number of migrated cells by
281 1.5-fold, as assessed by transwell migration (Fig. 2B). These findings demonstrate that miR-
282 409-3p inhibits angiogenic responses; whereas, its inhibition promotes angiogenic properties *in*
283 *vitro*.
284
285 To explore whether the miR-409-3p-mediated angiogenic responses could potentially impact
286 brown fat, we utilized an *in vitro* model in which 3T3-L1 fibroblasts were differentiated to a
287 brown-like phenotype (Supplemental Fig. 2A) and co-cultured with supernatant from HUVECs
288 transfected with either NS_m and miR-409_m (overexpressing miR-409-3p) or NS_i and miR-409_i
289 (inhibiting miR-409-3p) (Fig. 3A). Co-culture with supernatant from HUVECs transfected with
290 miR-409-$3p_m$ compared with non-specific control (NS_m) revealed reductions in expression for
291 uncoupling protein 1 (UCP1) by 78%, cell-death inducing DNA fragmentation factor-like effector
292 A (CIDEA) by 50% (Fig. 3B), peroxisome proliferator-activated receptor gamma co-activator 1-
293 alpha (PGC1α) by 25% (Supplemental Fig. 2B), and a 2.5-fold increase in ADIPOQ expression
294 (Supplemental Fig. 2C), as assessed by RT-qPCR. Additionally, co-culture from supernatants
295 from miR-409-3p overexpression in HUVECs reduced UCP1 and CIDEA protein expression by
296 25% and 37%, respectively (Fig. 3D). This decreased “browning” phenotype was further

supported by a 75% reduction in Oil Red O (ORO) staining for lipid droplets (Fig. 3F). In contrast, co-culture of 3T3-L1 cells with supernatants from HUVECs transfected with miR-409_i increased mRNA expression of browning markers: UCP1 (~2.16-fold; Fig. 3C), CIDEA (~1.46-fold; Fig. 3C), PGC1α (1.54-fold; Supplemental Fig. 2D), and decreased Adiponectin (ADIPOQ) expression (21%; Supplemental Fig. 2E). Furthermore, protein expression increased for UCP1 by 1.74-fold and for CIDEA by 1.56-fold (Fig. 3E). The increased "browning" phenotype exhibited by these differentiated adipocytes was further corroborated by a 1.4-fold increase in lipid droplets by ORO staining (Fig. 3G). Overall, these findings indicate that miR-409-3p may play a significant role in the differentiation state of adipocytes towards white or brown fat.

To ascertain if altering miR-409-3p expression could similarly regulate browning of human adipocytes, we used a complementary *ex vivo* approach, in which human punch biopsies were obtained from discarded subcutaneous adipose tissue after surgical removal and placed in culture for 7 days as organoids (Supplemental Fig. 3A). During this differentiation process, adipocyte samples were co-cultured with supernatants of ECs transfected with either NS_m and miR-409-$3p_m$ or NS_i and miR-409-$3p_i$. When co-cultured with miR-409-$3p_m$ supernatants, adipocytes demonstrated a reduction in brown fat mRNA markers, UCP1 (53%), CIDEA (71%), and PGC1-α (49%) (Supplemental Fig. 3B), and reduced expression of UCP1 (54%) and CD31 (47%) by immunofluorescence staining (Supplemental Fig. 3D). In contrast, organoids co-cultured with miR-409_i supernatants increased browning mRNA markers for UCP1 (1.93-fold), CIDEA (2.85-fold), and PGC1-α (3.1-fold) (Supplemental Fig. 3C). This phenotype was further supported by increased expression of UCP1 (3.9-fold) and CD31 (1.9-fold) using immunofluorescence staining (Supplemental Fig. 3E). Taken together, this data shows that miR-409-3p regulates adipocyte browning in both mouse and human cells.

We utilized an *in silico* approach to identify the target genes of miR-409-3p through the use of prediction algorithms (miRWalk, MicroT4, RNAhybrid, and TargetScan). Expression of the

324 predicted candidate genes targeting the 3'-UTR of miR-409-3p was validated on the mRNA and
325 protein levels. From 127 genes that were predicted by 5 prediction algorithms, the mRNA of 12
326 genes were decreased in HUVECs overexpressing miR-409-3p, and only 2 genes, ZEB1 and
327 MAP4K3, showed consistently reduced gene expression by Western Blot and enrichment in the
328 Myc-AGO2 complex (Figure 4A and data not shown). Overexpression of miR-409-3p
329 significantly decreased the mRNA expression of ZEB1 (~54%) and MAP4K3 (~66%) (Fig. 4B) in
330 HUVECs and in human sWAT organoids (Supplemental Fig. 4A). We also observed a
331 significant decrease in protein expression of ZEB1 (~42%) and MAP4K3 (~48%) (Fig. 4C) in
332 HUVECs. Conversely, inhibition of miR-409-3p increased the protein expression of ZEB1
333 (~1.34-fold) and MAP4K3 (~1.38-fold) (Fig. 4D). MiR-409-3p overexpression also inhibited
334 ZEB1 by 43% and MAP4K3 by 45% in 3'-UTR reporter assays (Fig. 4E). In contrast, miR-409-
335 3p inhibition led to a 1.28-fold increase in ZEB1 and 1.22-fold increase in MAP4K3 3'-UTR
336 reporter activities (Fig. 4F). Additionally, we observed a significant increase in mRNA
337 expression of ZEB1 and MAP4K3 in human sWAT organoids in response to miR-409-3p
338 inhibition (Supplemental Fig. 4B). Binding sites to ZEB1 and MAP4K3 3'UTR for miR-409-3p
339 were mapped by Rna22 (Supplemental Fig. 5A-B). To further verify that miR-409-3p directly
340 targets ZEB1 and MAP4K3 in ECs, we performed Argonaute2 (AGO2) microribonucleoprotein
341 IP (miRNP-IP) studies to assess whether ZEB1 and MAP4K3 mRNA is enriched in the RNA-
342 induced silencing complex following miR-409-3p overexpression in HUVECs. We observed
343 1.37-fold enrichment of ZEB1 and 1.56-fold enrichment of MAP4K3 mRNA following AGO2
344 miRNP-IP as compared to the miRNA-negative control (Fig. 4G). Finally, AGO2 miRNP-IP did
345 not enrich SMAD1, a gene that was not found to be a target of miR-409-3p (Supplemental Fig.
346 5C).
347
348 To evaluate whether neutralization of ZEB1 and MAP4K3 can "phenocopy" miR-409-3p
349 functional effects in ECs, we undertook siRNA-mediated knockdown approaches (Supplemental
350 Fig. 5D-E). Silencing of either ZEB1 or MAP4K3 significantly reduced EC proliferation by ~47%

351 and ~35%, respectively, as measured by BrdU incorporation (Fig. 5A and 5D), transwell
352 migration of ZEB1 by ~50% and MAP4K3 by ~25% (Fig. 5B and 5E) and wound closure by
353 ~43% and ~53%, respectively, in scratch assays (Fig. 5C and 5F). Interestingly, concurrent
354 silencing of ZEB1 and MAP4K3 showed cooperative effects on EC proliferation (27% compared
355 to $ZEB1_{siRNA}$ or $MAP4K3_{siRNA}$ alone) (Fig. 5G) and migration (85% compared to $ZEB1_{siRNA}$ or
356 $MAP4K3_{siRNA}$ alone) (Fig. 5H). In the absence of ZEB1 or MAP4K3, miR-409-3p overexpression
357 impaired EC proliferation demonstrating that miR-409-3p-mediated effects are partially
358 dependent on ZEB1 and MAP4K3 (Fig. 5I). Altogether, this data demonstrates ZEB1 and
359 MAP4K3 are *bone fide* targets of miR-409-3p in ECs, where increased levels of miR-409-3p in
360 ECs may potentially act as a molecular switch inhibiting EC growth and angiogenesis.
361
362 To assess whether miR-409-3p impacts adipocyte browning in a paracrine manner, we used
363 multiplex ELISA from the conditioned media of ECs overexpressing or deficient in miR-409-3p
364 and identified that the secretion of PLGF was significantly regulated by miR-409-3p.
365 Overexpression of miR-409-3p decreased PLGF secretion by ~46% (Fig. 6A); whereas, its
366 neutralization increased PLGF secretion by 7-fold (Fig. 6B). In contrast, EC secretion of EGF,
367 BMP-9, or VEGF-A were not regulated under these conditions (Fig. 6A-B). Interestingly, we
368 found that PLGF stimulation of 3T3-L1 cells during differentiation significantly increased UCP1
369 expression (Fig 6C). Additionally, knockdown of miR-409-3p coupled with PLGF stimulation
370 demonstrated greater UCP1 expression compared to PLGF stimulation alone (Fig. 6D). SiRNA-
371 mediated knockdown of miR-409-3p target genes, ZEB1 or MAP4K3, phenocopied miR-409-3p
372 effects on PLGF secretion and reduced EC secretion of PLGF (Fig. 6E). While siRNA mediated
373 knockdown of FLT1 in 3T3-L1 cells (Supplemental Fig. 6A) significantly reduced PLGF induced
374 UCP1 expression (Supplemental Fig. 6B). Taken together, this data suggests that the miR-409-
375 3p-mediated regulation of ZEB1 and MAP4K3 regulates PLGF release from ECs and browning
376 of 3T3-L1 adipocytes through FLT1.
377

378 To evaluate whether neutralization of miR-409-3p regulates angiogenesis and insulin resistance
379 in obese mice, LNA-miR-409-3p$_{inh}$ was delivered intravenously (i.v.) weekly in mice fed a HFD
380 (Fig. 7A). LNA-miR-409-3p$_{inh}$ decreased miR-409-3p expression ~22% in the EC of BAT
381 following only two i.v. injections compared to the LNA-NS$_{inh}$ control group (Supplementary Fig.
382 7A). Although body weights and composition did not significantly change between LNA-NS$_{inh}$
383 and the LNA-miR-409-3p$_{inh}$ groups over 15 weeks of HFD (Fig. 7B and Supplemental Table 2),
384 insulin (ITT) (Fig. 7C) and glucose (GTT) (Fig. 7D) tolerance and energy expenditure (Fig. 7E
385 and Supplementary Fig. 7B) were significantly improved in response to miR-409-3p
386 neutralization. There were no significant differences in locomotor activity, food intake
387 (Supplemental Fig. 7C-D) or the whole body fat distribution (Supplemental Table 2), while the
388 respiratory exchange rate (RER) was significantly decreased (Supplemental Fig. 7E).
389 Remarkably, inhibition of miR-409-3p induced angiogenesis as measured by CD31 ~2.4-fold
390 (Fig. 7F) and increased UCP1, while decreasing adipocyte size (Fig. 7G). Collectively, these
391 findings indicate that miR-409-3p is not only an anti-angiogenic miRNA, but may also contribute
392 to the activation of a metabolic program in mice with obesity.
393

394 **Discussion**

395 The function of BAT is dependent on its proper vascularization that is tightly regulated by a
396 range of cytokines and angiogenic factors. However, the precise factors involved in this EC-
397 adipocyte crosstalk are poorly understood. There are many pathological changes that occur in
398 obesity, including EC dysfunction and impaired angiogenesis in adipose depots. Long-term HFD
399 triggers 'whitening' of BAT that is characterized by reduced expression of mitochondria-
400 associated genes, such as UCP1, increased lipid deposition, enlargement of lipid droplets,
401 elevated mitochondrial ROS production, and membrane depolarization [22, 48]. In this study, we
402 delineate the molecular mechanisms by which miR-409-3p deficiency regulates EC-driven
403 angiogenesis and, in turn, improves BAT browning, insulin resistance, and metabolic
404 parameters in obesity.

405

406 Accumulating studies demonstrate that microRNAs contribute to BAT functionality. In response
407 to prolonged cold exposure, expression of miR-193a/b [49], miR-365 [49], miR-30b/c [50] and
408 miR-455 [51] were upregulated both in human and mouse BAT. Overexpression of these
409 miRNAs in mice promoted brown adipocyte cell differentiation and browning of sWAT.
410 Conversely, the miR-27 family negatively regulated BAT both in mice [52] and human subjects
411 [53]. Our study adds a new layer to these findings by demonstrating how neutralization of a
412 miRNA, miR-409-3p, improves angiogenic responses and metabolic functionality in BAT
413 through EC-adipocyte crosstalk. Interestingly, the metabolic benefits we observed in this study,
414 including improved glucose and insulin tolerance and increased energy expenditure, did not
415 correlate into a lower body weight in obese mice with miR-409-3p neutralization. It is likely that
416 systemic neutralization of miR-409-3p and associated stimulation of angiogenesis may have
417 contributed to expansion of the WAT in addition to restoring BAT function and thereby inhibiting
418 weight loss in response to miR-409-3p neutralization. In fact, body composition analyses
419 showed a non-significant increased trend in total weight and visceral and subcutaneous adipose
420 weights (Supplemental Table 2). Whether inhibition of miR-409-3p promotes angiogenesis in
421 other peripheral tissues that could potentially contribute to the improved insulin sensitivity
422 observed in these mice remains a possibility and will be of interest to explore in future studies.
423

424 In the overall response to metabolic changes, cell-to-cell communication plays a fundamental
425 role [54]. Through *in vitro* co-culture techniques [55, 56], healthy adipocytes exhibit decreased
426 insulin sensitivity and elevated inflammatory markers when exposed to ECs from obese
427 patients; thereby, revealing the importance of cytokines, such as IL-6 and IL-1β, in the crosstalk
428 between adipocytes and visceral adipose ECs [57]. Emerging studies demonstrate that
429 decreasing inflammation in the microvasculature may favorably delay the development of insulin
430 resistance [36]. Our findings build upon these paracrine mechanisms, demonstrating how miR-
431 409-3p stimulated EC secretion of the pro-angiogenic factor, PLGF (Supplemental Fig. 8).

432 Endothelial cell characteristics in the microvasculature of adipose depots can be different than
433 the HUVECs that were used in our co-culture studies and the use microvascular endothelial
434 cells could reflect a more relevant model system. In addition, although *in vitro* aspects of our
435 study mostly focused on the modulation of browning during pre-adipocyte differentiation our *ex*
436 *vivo studies* with human sWAT organoids and *in vivo* studies in obese mice gave insights into
437 the ability of miR-409-3p regulate browning in mature adipocytes.
438
439 MAP4K3 has a well-established role in cell growth, proliferation, and migration in various cell
440 lines. Overexpression of MAP4K3 in HeLa cells induces the activation of mTOR downstream
441 signaling molecules, S6K and 4E-BP1, in response to changes in nutrient and energy levels. In
442 contrast, knockdown of MAP4K3 inhibits growth of HeLa cells [58]. Overexpression of MAP4K3
443 induces cell proliferation through the activation of the NF-κB pathway in primary human
444 hepatocytes [59]. Whole-body MAP4K3 transgenic mice exhibited higher migration of primary
445 lung epithelial cells that promoted metastasis through IQGAP1 phosphorylation [60]. Our
446 findings demonstrating how the knockdown of MAP4K3 has an inhibitory effect on EC growth
447 and migration are in agreement with the literature findings (Fig. 5). We also demonstrated a
448 novel role for MAP4K3, where its modulation in ECs regulates PLGF secretion, contributing to
449 adipose browning (Fig. 6).
450
451 ZEB1 knockdown also significantly inhibited EC growth, migration, and endothelial PLGF
452 release (Fig. 5 and 6). ZEB1 is central transcriptional component of fat cell differentiation with
453 higher expression levels in pre-adipocytes compared to the mature adipocytes [61]. It controls
454 adipogenesis both in committed 3T3-L1 cells, as well as in mesenchymal stem cells (MSCs)
455 through cooperating with C/EBPβ [61]. Although our study focused on the regulation of ZEB1
456 through miR-409-3p in ECs *in vitro* and *in vivo*, we cannot completely rule out the systemic
457 effect of miR-409-3p neutralization and ZEB1 regulation in our *in vivo* studies.
458

459 Previously, miR-409-3p was shown to regulate metastasis in human breast cancer cells through
460 targeting ZEB1 [62]. Contradictory to these findings, a recent study showed that in
461 osteosarcoma cells, miR-409-3p acts as a tumor suppressor through negatively regulating
462 ZEB1 [63]. Our study brings in a novel component to these previous findings where the miR-
463 409-3p-MAP4K3/ZEB1 signaling axis regulates PLGF release from ECs; therefore, linking
464 PLGF to downstream regulation of adipose browning. However, further studies are needed to
465 uncover the exact mechanism by which MAP4K3/ZEB1 regulate PLGF and other pro-
466 angiogenic factors (Supplemental Fig. 8).
467
468 In summary, we identified that miR-409-3p expression is increased in BAT ECs of obese mice
469 and in human subjects with diabetes. MiR-409-3p serves as a negative regulator of EC
470 angiogenesis and adipose browning through targeting ZEB1 and MAP4K3; thereby, in turn,
471 regulating the EC secretion of PLGF. Additionally, inhibition of miR-409-3p markedly increased
472 BAT angiogenesis, improved insulin resistance, and stimulated adipose browning in a mouse
473 model of DIO. Therapies focusing on neutralization of miR-409-3p, or its downstream signaling
474 pathways, may offer a new strategy to promote BAT neovascularization and improve metabolic
475 phenotypes in obesity.

476 **Figure Legends**

477

478 **Fig. 1** MicroRNA-409-3p (MiR-409-3p) discovery in mice and human diabetic models and its
479 regulation of EC growth *in-vitro*. **a** Workflow of genome wide RNA-seq profiling for the
480 identification of miR-409-3p using ECs from BAT. **b** MiR-409-3p expression in BAT of mice
481 placed on chow or HF diet for 8 weeks. **c** Expression of miR-409-3p in HUAECs, preadipocytes,
482 adipocytes, splenic (sp) derived monocytes, bone marrow (BM) derived monocytes, and
483 fibroblasts compared to human umbilical vein endothelial cells (HUVEC). **d** miR-409-3p
484 overexpressed or **e** knocked down in HUVECs and subjected to BrdU (5-bromo-2'-deoxyuridine)
485 cell proliferation assay. Data representative of n=3-6 per condition unless indicated otherwise.
486 All statistics calculated by student's t-test except for two-way ANOVA in 1d. $*p < 0.05$, $**p <$
487 0.01, $***p < 0.001$. Error bars indicate ± SEM

488

489 **Fig. 2** MiR-409-3p regulates EC migration. HUVECs transfected with non-specific control (NS_m)
490 or miR-409-3p mimic (miR-409-3p$_m$) (**a, c, e, g**) or miR-negative inhibitor control (NS_i) and miR-
491 409-3p inhibitor (miR-409-3p$_i$) (**b, d, f, h**) were subjected to **a, b** EC migration in transwell
492 Boyden chambers; **c, d** scratch assay (Scale bars, 100 µm); **e, f** spheroid formation assay
493 (Scale bars, 100 µm); **g, h** matrigel tube formation assay (Scale bars, 40 µm). Data
494 representative of n=3-8 experiments. All statistics calculated by unpaired student's t-test or two-
495 way ANOVA, based on a comparison with respective control group. $*p < 0.05$, $**p < 0.01$, $***p <$
496 0.001. Error bars indicate ± SEM

497

498 **Fig. 3** MiR-409-3p differentiates 3T3-L1 fibroblasts into brown-like adipocytes. Supernatant from
499 HUVECs 3 days post-transfection with NS_m/miR-409-3p$_m$ or NS_i/miR-409-3p$_i$ were cultured with
500 3T3-L1 fibroblasts for 4 days, followed by **a** RT-qPCR analysis of brown fat gene expression
501 (UCP1 and CIDEA) with either **b** mimic or **c** inhibitor, with results normalized to α-tubulin.
502 Western blot analyses for UCP1, CIDEA, and α-tubulin protein expression **d** and **e**, as well as

503 Oil-red O staining of 3T3-L1 cells **f** and **g**. Data representative of n=3-9 experiments. All
504 statistics calculated by unpaired student's t-test or two-way ANOVA, based on a comparison
505 with respective non-specific control group. $*p < 0.05$, $**p < 0.01$, $***p < 0.001$. Error bars
506 indicate ± SEM
507
508 **Fig. 4** ZEB1 and MAP4K3 are potential targets of miR-409-3p. **a** Overall workflow used for
509 target identification. HUVECs were either transfected with (**b, c, e, g**) NS_m and miR-409-$3p_m$ or
510 **d** and **f** NS_i and miR-409-$3p_i$, followed by **b** RT-qPCR analysis of ZEB1 and MAP4K3 mRNA
511 expression. Total of n=3 experiments. **c** and **d** Western blot analyses for ZEB1, MAP4K3, and
512 β-actin protein expression. Protein blots representative of n=3-4 experiments. **e** and **f** Luciferase
513 activity (RLU) of ZEB1 and MAP4K3 3'-untranslated regions (UTRs) normalized to total protein.
514 Data representative of n=3-6 experiments. **g** RNA co-precipitation (co-IP) conducted using
515 ZEB1 and MAP4K3, normalized to Myc and HPRT. n=3 per condition. All statistics calculated by
516 unpaired student's t-test or two-way ANOVA, based on a comparison with respective non-
517 specific control group. $*p < 0.05$, $**p < 0.01$, $***p < 0.001$. Error bars indicate ± SEM
518
519 **Fig. 5** SiRNA-mediated knockdown of zinc finger E-box-binding homeobox 1 (ZEB1) and
520 mitogen-activated protein kinase kinase kinase kinase 3 (MAP4K3) recapitulates miR-409-3p
521 functional effects in endothelial cells (ECs). Human umbilical vein ECs (HUVECs) were
522 transfected with siRNA to (**a-c, g, h, i**) ZEB1, (**d-i**) MAP4K3, or scrambled control (ctrl). EC
523 proliferation was then determined by (**a, d, g, i**) BrdU assay. Migration of ECs was quantified by
524 either (**c, f**) scratch assay or (**b, e, h**) transwell Boyden chambers. **g** and **h** SiRNA to ZEB1 and
525 MAP4K3 was included to assess for combinatorial effects. **i** NS_m and miR-409-$3p_m$ were
526 transfected in order to assess dependency. Scale bars, 100 μm. Data representative of n=3-6
527 experiments. All statistics calculated by unpaired student's t-test or two-way ANOVA, based on
528 a comparison with indicated control group. $*p < 0.05$, $**p < 0.01$, $***p < 0.001$. Error bars
529 indicate ± SEM

530 **Fig. 6** MiR-409-3p regulates the secretion of PLGF and 3T3-L1 browning. **a** and **b** Conditioned
531 media from HUVECs were transfected with **a** NS_m/miR-409-3p_m or **b** NS_i/miR-409-3p_i and
532 subjected to multiplex ELISA. **a** and **b** Secreted PLGF, EGF, BMP9, and VEGF-A were
533 quantified using the multiplex ELISA. **c** Stimulation of 3T3-L1 cells with 100 or 150 ng/mL PLGF
534 or vehicle control increased UCP1 expression as measured by RT-qPCR. **d** Conditioned media
535 from HUVECs transfected with NS_i or miR-409-3p_i were added to 3T3-L1 cells in the presence
536 or absence of PLGF (200 ng/mL) and UCP1 expression was quantified by RT-qPCR. **e**
537 Conditioned media from HUVECs transfected with scrambled control siRNA ($Cntrl_{siRNA}$),
538 $ZEB1_{siRNA}$, or $MAP4K3_{siRNA}$ was subjected to ELISA to measure secreted PLGF release. All RT-
539 qPCR results normalized to 36B4 as the housekeeping gene. All statistics calculated by (**a-c, e**)
540 unpaired student's t-test or (**d**) two-way ANOVA, based on a comparison with indicated control
541 group. *$p < 0.05$, **$p < 0.01$, ***$p < 0.001$. Error bars indicate ± SEM
542
543 **Fig. 7** MiR-409-3p neutralization stimulates BAT angiogenesis and improves insulin resistance
544 and energy expenditure in obese mice. **a** and **b** C57BL/6J mice fed high-fat diet (HFD) were
545 intravenously (i.v.) injected with vehicle non-specific control (LNA-NSi) or LNA-miR-409-3p
546 inhibitor (LNA-409-3pi) at 10 mg/kg for 15 weeks. **c** At 13 weeks, mice were subjected to insulin
547 tolerance test (ITT) via i.v. injection with 0.75 U/kg insulin. **d** At 14 weeks, glucose tolerance test
548 (GTT) was performed using 1 U/kg glucose. **e-g** Metabolic caging studies over a two-day period
549 (2 light and 2 dark cycles) were performed after 15 weeks and **e** energy expenditure (EE)
550 quantified. Immunofluorescence staining for **f** CD31/DAPI, **g** UCP1/perilipin (PLIN1)/DAPI was
551 quantified in brown adipose tissue from the indicated mice. Total of 10 animals per group were
552 used. All statistics calculated by unpaired student's t-test based on a comparison with
553 respective control group. *$p < 0.05$, **$p < 0.01$, ***$p < 0.001$. Error bars indicate ± SEM
554
555
556

Funding: This work was supported by the American Diabetes Association grant #1-16-JDF-046 (to B.I.), a Behrakis Junior Faculty Development Award (to B.I.), a Watkins Discovery Award (to B.I.), a National Institutes of Health (HL149999 to B.I.), a National Institutes of Health (HL115141, HL134849, HL148207, HL148355, HL153356 to M.W.F), an American Heart Association grant (18SFRN33900144 and 20SFRN35200163 to M.W.F.), the Arthur K. Watson Charitable Trust (to M.W.F).

Author Contributions

MWF and BI designed research; BI, DBG, HL, DPC, WW, FB and DOz, carried out the experiments; DO, contributed critical reagents; DBG, HL, DPC, WW, FB, MWF and BI analyzed and interpreted the data; and DBG, MWF and BI wrote the manuscript

Acknowledgments: We thank Lay-Hong Ang and Aniket Gad for Confocal Microscopy technical assistance (NIH P30DK034854), Yevgenia Tesmenitsky for her assistance with i.v. injections, Merve Kurt with her technical assistance in EC scratch assays and Carolyn Niosi for her technical assistance in cell culture.

Conflict of interest

The authors have declared that no conflict of interest exists with this work.

References

592 1. Saltiel AR, Olefsky JM. Inflammatory mechanisms linking obesity and metabolic
593 disease. J Clin Invest. 2017;127(1):1-4. doi: 10.1172/JCI92035.
594 2. Dall TM, Yang W, Halder P, Pang B, Massoudi M, Wintfeld N, et al. The economic
595 burden of elevated blood glucose levels in 2012: diagnosed and undiagnosed diabetes,
596 gestational diabetes mellitus, and prediabetes. Diabetes Care. 2014;37(12):3172-9. doi:
597 10.2337/dc14-1036.
598 3. American Diabetes A. Economic costs of diabetes in the U.S. in 2012. Diabetes Care.
599 2013;36(4):1033-46. doi: 10.2337/dc12-2625.
600 4. Swinburn BA, Sacks G, Hall KD, McPherson K, Finegood DT, Moodie ML, et al. The
601 global obesity pandemic: shaped by global drivers and local environments. Lancet.
602 2011;378(9793):804-14. doi: 10.1016/S0140-6736(11)60813-1.
603 5. Smorlesi A, Frontini A, Giordano A, Cinti S. The adipose organ: white-brown
604 adipocyte plasticity and metabolic inflammation. Obes Rev. 2012;13 Suppl 2:83-96. doi:
605 10.1111/j.1467-789X.2012.01039.x.
606 6. Cypess AM, Lehman S, Williams G, Tal I, Rodman D, Goldfine AB, et al.
607 Identification and importance of brown adipose tissue in adult humans. N Engl J Med.
608 2009;360(15):1509-17. doi: 10.1056/NEJMoa0810780.
609 7. Virtanen KA, Lidell ME, Orava J, Heglind M, Westergren R, Niemi T, et al. Functional
610 brown adipose tissue in healthy adults. N Engl J Med. 2009;360(15):1518-25. doi:
611 10.1056/NEJMoa0808949.
612 8. Saito M, Okamatsu-Ogura Y, Matsushita M, Watanabe K, Yoneshiro T, Nio-
613 Kobayashi J, et al. High incidence of metabolically active brown adipose tissue in
614 healthy adult humans: effects of cold exposure and adiposity. Diabetes.
615 2009;58(7):1526-31. doi: 10.2337/db09-0530.
616 9. Crewe C, An YA, Scherer PE. The ominous triad of adipose tissue dysfunction:
617 inflammation, fibrosis, and impaired angiogenesis. J Clin Invest. 2017;127(1):74-82. doi:
618 10.1172/JCI88883.
619 10. Olsson AK, Dimberg A, Kreuger J, Claesson-Welsh L. VEGF receptor signalling - in
620 control of vascular function. Nat Rev Mol Cell Biol. 2006;7(5):359-71. doi:
621 10.1038/nrm1911.
622 11. Rausch ME, Weisberg S, Vardhana P, Tortoriello DV. Obesity in C57BL/6J mice is
623 characterized by adipose tissue hypoxia and cytotoxic T-cell infiltration. Int J Obes
624 (Lond). 2008;32(3):451-63. doi: 10.1038/sj.ijo.0803744.
625 12. Yin J, Gao Z, He Q, Zhou D, Guo Z, Ye J. Role of hypoxia in obesity-induced
626 disorders of glucose and lipid metabolism in adipose tissue. Am J Physiol Endocrinol
627 Metab. 2009;296(2):E333-42. doi: 10.1152/ajpendo.90760.2008.
628 13. Sun K, Wernstedt Asterholm I, Kusminski CM, Bueno AC, Wang ZV, Pollard JW, et
629 al. Dichotomous effects of VEGF-A on adipose tissue dysfunction. Proc Natl Acad Sci U
630 S A. 2012;109(15):5874-9. doi: 10.1073/pnas.1200447109.
631 14. Gealekman O, Guseva N, Hartigan C, Apotheker S, Gorgoglione M, Gurav K, et al.
632 Depot-specific differences and insufficient subcutaneous adipose tissue angiogenesis in
633 human obesity. Circulation. 2011;123(2):186-94. doi:
634 10.1161/CIRCULATIONAHA.110.970145.
635 15. O'Rourke RW, White AE, Metcalf MD, Olivas AS, Mitra P, Larison WG, et al.
636 Hypoxia-induced inflammatory cytokine secretion in human adipose tissue
637 stromovascular cells. Diabetologia. 2011;54(6):1480-90. doi: 10.1007/s00125-011-
638 2103-y.

639 16. Cao Y. Adipose tissue angiogenesis as a therapeutic target for obesity and
640 metabolic diseases. Nat Rev Drug Discov. 2010;9(2):107-15. doi: 10.1038/nrd3055.
641 17. Folkman J. Angiogenesis. Annu Rev Med. 2006;57:1-18. doi:
642 10.1146/annurev.med.57.121304.131306.
643 18. Cheng R, Ma JX. Angiogenesis in diabetes and obesity. Rev Endocr Metab Disord.
644 2015;16(1):67-75. doi: 10.1007/s11154-015-9310-7.
645 19. Hausman GJ, Richardson RL. Adipose tissue angiogenesis. J Anim Sci.
646 2004;82(3):925-34. doi: 10.2527/2004.823925x.
647 20. Sun K, Kusminski CM, Luby-Phelps K, Spurgin SB, An YA, Wang QA, et al. Brown
648 adipose tissue derived VEGF-A modulates cold tolerance and energy expenditure.
649 Molecular metabolism. 2014;3(4):474-83. doi: 10.1016/j.molmet.2014.03.010.
650 21. Park J, Kim M, Sun K, An YA, Gu X, Scherer PE. VEGF-A-Expressing Adipose
651 Tissue Shows Rapid Beiging and Enhanced Survival After Transplantation and Confers
652 IL-4-Independent Metabolic Improvements. Diabetes. 2017;66(6):1479-90. doi:
653 10.2337/db16-1081.
654 22. Shimizu I, Aprahamian T, Kikuchi R, Shimizu A, Papanicolaou KN, MacLauchlan S,
655 et al. Vascular rarefaction mediates whitening of brown fat in obesity. J Clin Invest.
656 2014;124(5):2099-112. doi: 10.1172/JCI71643.
657 23. Stanford KI, Middelbeek RJ, Townsend KL, An D, Nygaard EB, Hitchcox KM, et al.
658 Brown adipose tissue regulates glucose homeostasis and insulin sensitivity. J Clin
659 Invest. 2013;123(1):215-23. doi: 10.1172/JCI62308.
660 24. Ye J, Gao Z, Yin J, He Q. Hypoxia is a potential risk factor for chronic inflammation
661 and adiponectin reduction in adipose tissue of ob/ob and dietary obese mice. Am J
662 Physiol Endocrinol Metab. 2007;293(4):E1118-28. doi: 10.1152/ajpendo.00435.2007.
663 25. He Q, Gao Z, Yin J, Zhang J, Yun Z, Ye J. Regulation of HIF-1{alpha} activity in
664 adipose tissue by obesity-associated factors: adipogenesis, insulin, and hypoxia. Am J
665 Physiol Endocrinol Metab. 2011;300(5):E877-85. doi: 10.1152/ajpendo.00626.2010.
666 26. Kendall RL, Thomas KA. Inhibition of vascular endothelial cell growth factor activity
667 by an endogenously encoded soluble receptor. Proc Natl Acad Sci U S A.
668 1993;90(22):10705-9. doi: 10.1073/pnas.90.22.10705.
669 27. Autiero M, Waltenberger J, Communi D, Kranz A, Moons L, Lambrechts D, et al.
670 Role of PlGF in the intra- and intermolecular cross talk between the VEGF receptors
671 Flt1 and Flk1. Nat Med. 2003;9(7):936-43. doi: 10.1038/nm884.
672 28. Dewerchin M, Carmeliet P. PlGF: a multitasking cytokine with disease-restricted
673 activity. Cold Spring Harb Perspect Med. 2012;2(8). doi: 10.1101/cshperspect.a011056.
674 29. Lijnen HR, Christiaens V, Scroyen I, Voros G, Tjwa M, Carmeliet P, et al. Impaired
675 adipose tissue development in mice with inactivation of placental growth factor function.
676 Diabetes. 2006;55(10):2698-704. doi: 10.2337/db06-0526.
677 30. Hemmeryckx B, van Bree R, Van Hoef B, Vercruysse L, Lijnen HR, Verhaeghe J.
678 Adverse adipose phenotype and hyperinsulinemia in gravid mice deficient in placental
679 growth factor. Endocrinology. 2008;149(5):2176-83. doi: 10.1210/en.2007-1272.
680 31. Karolina DS, Armugam A, Sepramaniam S, Jeyaseelan K. miRNAs and diabetes
681 mellitus. Expert Rev Endocrinol Metab. 2012;7(3):281-300. doi: 10.1586/eem.12.21.
682 32. Chamorro-Jorganes A, Araldi E, Suarez Y. MicroRNAs as pharmacological targets
683 in endothelial cell function and dysfunction. Pharmacol Res. 2013;75:15-27. doi:
684 10.1016/j.phrs.2013.04.002.
685 33. Arner P, Kulyte A. MicroRNA regulatory networks in human adipose tissue and
686 obesity. Nat Rev Endocrinol. 2015;11(5):276-88. doi: 10.1038/nrendo.2015.25.

687 34. Chartoumpekis DV, Zaravinos A, Ziros PG, Iskrenova RP, Psyrogiannis AI,
688 Kyriazopoulou VE, et al. Differential expression of microRNAs in adipose tissue after
689 long-term high-fat diet-induced obesity in mice. PLoS One. 2012;7(4):e34872. doi:
690 10.1371/journal.pone.0034872.
691 35. Guller I, McNaughton S, Crowley T, Gilsanz V, Kajimura S, Watt M, et al.
692 Comparative analysis of microRNA expression in mouse and human brown adipose
693 tissue. BMC Genomics. 2015;16:820. doi: 10.1186/s12864-015-2045-8.
694 36. Sun X, Lin J, Zhang Y, Kang S, Belkin N, Wara AK, et al. MicroRNA-181b Improves
695 Glucose Homeostasis and Insulin Sensitivity by Regulating Endothelial Function in
696 White Adipose Tissue. Circ Res. 2016;118(5):810-21. doi:
697 10.1161/CIRCRESAHA.115.308166.
698 37. Frost RJ, Olson EN. Control of glucose homeostasis and insulin sensitivity by the
699 Let-7 family of microRNAs. Proc Natl Acad Sci U S A. 2011;108(52):21075-80. doi:
700 10.1073/pnas.1118922109.
701 38. Jordan SD, Kruger M, Willmes DM, Redemann N, Wunderlich FT, Bronneke HS, et
702 al. Obesity-induced overexpression of miRNA-143 inhibits insulin-stimulated AKT
703 activation and impairs glucose metabolism. Nat Cell Biol. 2011;13(4):434-46. doi:
704 10.1038/ncb2211.
705 39. Trajkovski M, Hausser J, Soutschek J, Bhat B, Akin A, Zavolan M, et al. MicroRNAs
706 103 and 107 regulate insulin sensitivity. Nature. 2011;474(7353):649-53. doi:
707 10.1038/nature10112.
708 40. Karamanlidis G, Karamitri A, Docherty K, Hazlerigg DG, Lomax MA. C/EBPbeta
709 reprograms white 3T3-L1 preadipocytes to a Brown adipocyte pattern of gene
710 expression. The Journal of biological chemistry. 2007;282(34):24660-9. doi:
711 10.1074/jbc.M703101200.
712 41. Ohno H, Shinoda K, Spiegelman BM, Kajimura S. PPARgamma agonists induce a
713 white-to-brown fat conversion through stabilization of PRDM16 protein. Cell metabolism.
714 2012;15(3):395-404. doi: 10.1016/j.cmet.2012.01.019.
715 42. Liu P, Huang S, Ling S, Xu S, Wang F, Zhang W, et al. Foxp1 controls brown/beige
716 adipocyte differentiation and thermogenesis through regulating beta3-AR
717 desensitization. Nature communications. 2019;10(1):5070. doi: 10.1038/s41467-019-
718 12988-8.
719 43. Wara AK, Croce K, Foo S, Sun X, Icli B, Tesmenitsky Y, et al. Bone marrow-derived
720 CMPs and GMPs represent highly functional proangiogenic cells: implications for
721 ischemic cardiovascular disease. Blood. 2011;118(24):6461-4. doi: 10.1182/blood-
722 2011-06-363457.
723 44. Icli B, Wara AK, Moslehi J, Sun X, Plovie E, Cahill M, et al. MicroRNA-26a regulates
724 pathological and physiological angiogenesis by targeting BMP/SMAD1 signaling. Circ
725 Res. 2013;113(11):1231-41. doi: 10.1161/CIRCRESAHA.113.301780.
726 45. Sun X, Icli B, Wara AK, Belkin N, He S, Kobzik L, et al. MicroRNA-181b regulates
727 NF-kappaB-mediated vascular inflammation. J Clin Invest. 2012;122(6):1973-90. doi:
728 10.1172/JCI61495.
729 46. Fayyad AM, Khan AA, Abdallah SH, Alomran SS, Bajou K, Khattak MNK.
730 Rosiglitazone Enhances Browning Adipocytes in Association with MAPK and PI3-K
731 Pathways During the Differentiation of Telomerase-Transformed Mesenchymal Stromal
732 Cells into Adipocytes. Int J Mol Sci. 2019;20(7). doi: 10.3390/ijms20071618.

733 47. Halbgebauer D, Dahlhaus M, Wabitsch M, Fischer-Posovszky P, Tews D. Browning
734 capabilities of human primary adipose-derived stromal cells compared to SGBS cells.
735 Scientific reports. 2020;10(1):9632. doi: 10.1038/s41598-020-64369-7.
736 48. Alcala M, Calderon-Dominguez M, Bustos E, Ramos P, Casals N, Serra D, et al.
737 Increased inflammation, oxidative stress and mitochondrial respiration in brown adipose
738 tissue from obese mice. Sci Rep. 2017;7(1):16082. doi: 10.1038/s41598-017-16463-6.
739 49. Sun L, Xie H, Mori MA, Alexander R, Yuan B, Hattangadi SM, et al. Mir193b-365 is
740 essential for brown fat differentiation. Nat Cell Biol. 2011;13(8):958-65. doi:
741 10.1038/ncb2286.
742 50. Hu F, Wang M, Xiao T, Yin B, He L, Meng W, et al. miR-30 promotes thermogenesis
743 and the development of beige fat by targeting RIP140. Diabetes. 2015;64(6):2056-68.
744 doi: 10.2337/db14-1117.
745 51. Zhang H, Guan M, Townsend KL, Huang TL, An D, Yan X, et al. MicroRNA-455
746 regulates brown adipogenesis via a novel HIF1an-AMPK-PGC1alpha signaling network.
747 EMBO Rep. 2015;16(10):1378-93. doi: 10.15252/embr.201540837.
748 52. Sun L, Trajkovski M. MiR-27 orchestrates the transcriptional regulation of brown
749 adipogenesis. Metabolism. 2014;63(2):272-82. doi: 10.1016/j.metabol.2013.10.004.
750 53. Kang T, Lu W, Xu W, Anderson L, Bacanamwo M, Thompson W, et al. MicroRNA-
751 27 (miR-27) targets prohibitin and impairs adipocyte differentiation and mitochondrial
752 function in human adipose-derived stem cells. J Biol Chem. 2013;288(48):34394-402.
753 doi: 10.1074/jbc.M113.514372.
754 54. Crewe C, Joffin N, Rutkowski JM, Kim M, Zhang F, Towler DA, et al. An Endothelial-
755 to-Adipocyte Extracellular Vesicle Axis Governed by Metabolic State. Cell.
756 2018;175(3):695-708 e13. doi: 10.1016/j.cell.2018.09.005.
757 55. Bogdanowicz DR, Lu HH. Multifunction co-culture model for evaluating cell-cell
758 interactions. Methods Mol Biol. 2014;1202:29-36. doi: 10.1007/7651_2013_62.
759 56. Goers L, Freemont P, Polizzi KM. Co-culture systems and technologies: taking
760 synthetic biology to the next level. J R Soc Interface. 2014;11(96). doi:
761 10.1098/rsif.2014.0065.
762 57. Pellegrinelli V, Rouault C, Veyrie N, Clement K, Lacasa D. Endothelial cells from
763 visceral adipose tissue disrupt adipocyte functions in a three-dimensional setting: partial
764 rescue by angiopoietin-1. Diabetes. 2014;63(2):535-49. doi: 10.2337/db13-0537.
765 58. Findlay GM, Yan L, Procter J, Mieulet V, Lamb RF. A MAP4 kinase related to Ste20
766 is a nutrient-sensitive regulator of mTOR signalling. Biochem J. 2007;403(1):13-20. doi:
767 10.1042/BJ20061881.
768 59. Chuang HC, Lan JL, Chen DY, Yang CY, Chen YM, Li JP, et al. The kinase GLK
769 controls autoimmunity and NF-kappaB signaling by activating the kinase PKC-theta in T
770 cells. Nat Immunol. 2011;12(11):1113-8. doi: 10.1038/ni.2121.
771 60. Chuang HC, Chang CC, Teng CF, Hsueh CH, Chiu LL, Hsu PM, et al.
772 MAP4K3/GLK Promotes Lung Cancer Metastasis by Phosphorylating and Activating
773 IQGAP1. Cancer Res. 2019;79(19):4978-93. doi: 10.1158/0008-5472.CAN-19-1402.
774 61. Gubelmann C, Schwalie PC, Raghav SK, Roder E, Delessa T, Kiehlmann E, et al.
775 Identification of the transcription factor ZEB1 as a central component of the adipogenic
776 gene regulatory network. Elife. 2014;3:e03346. doi: 10.7554/eLife.03346.
777 62. Ma Z, Li Y, Xu J, Ren Q, Yao J, Tian X. MicroRNA-409-3p regulates cell invasion
778 and metastasis by targeting ZEB1 in breast cancer. IUBMB Life. 2016;68(5):394-402.
779 doi: 10.1002/iub.1494.

780 63. Wu L, Zhang Y, Huang Z, Gu H, Zhou K, Yin X, et al. MiR-409-3p Inhibits Cell
781 Proliferation and Invasion of Osteosarcoma by Targeting Zinc-Finger E-Box-Binding
782 Homeobox-1. Front Pharmacol. 2019;10:137. doi: 10.3389/fphar.2019.00137.
783

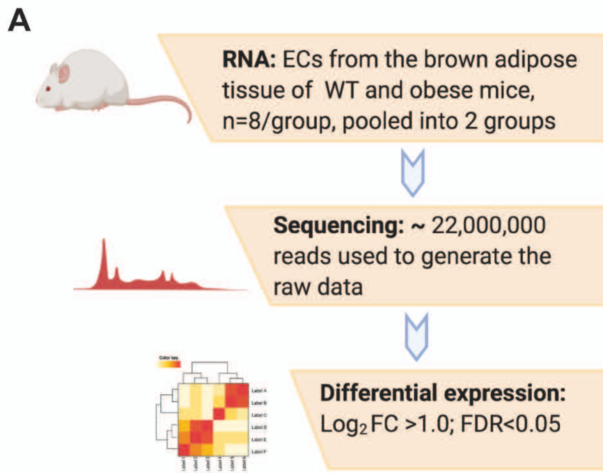
A
RNA: ECs from the brown adipose tissue of WT and obese mice, n=8/group, pooled into 2 groups
Sequencing: ~ 22,000,000 reads used to generate the raw data
Differential expression: Log2 FC >1.0; FDR<0.05

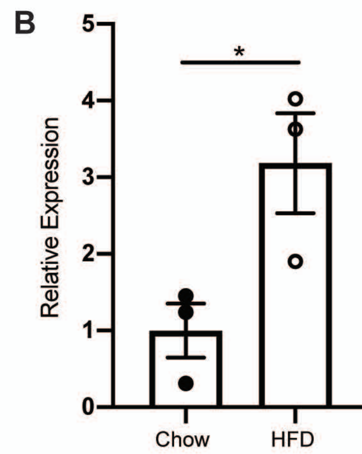
B
Relative Expression
Chow
HFD
*

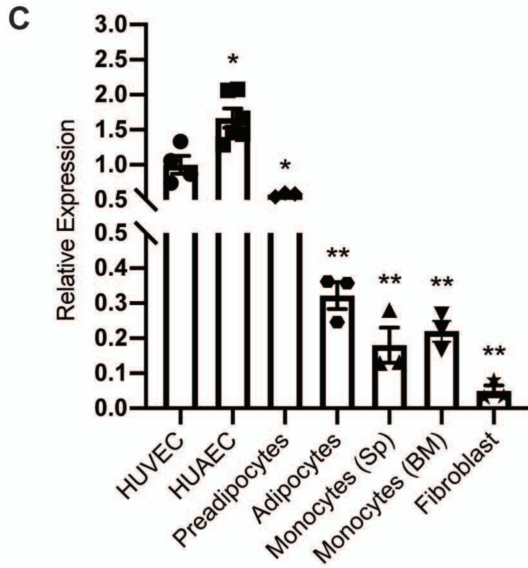
C
Relative Expression
HUVEC
HUAEC
Preadipocytes
Adipocytes
Monocytes (Sp)
Monocytes (BM)
Fibroblast

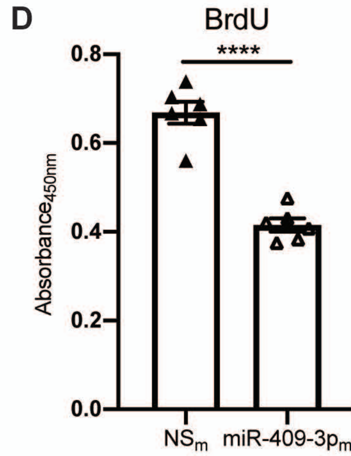
D
BrdU
Absorbance450nm
NSm
miR-409-3pm
****

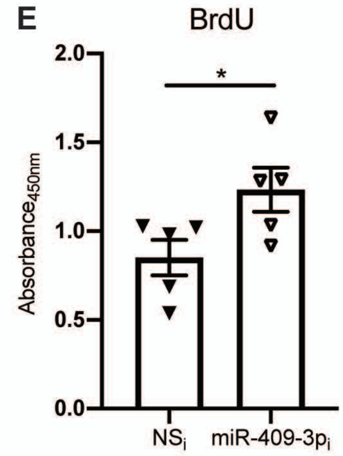
E
BrdU
Absorbance450nm
NSi
miR-409-3pi
*

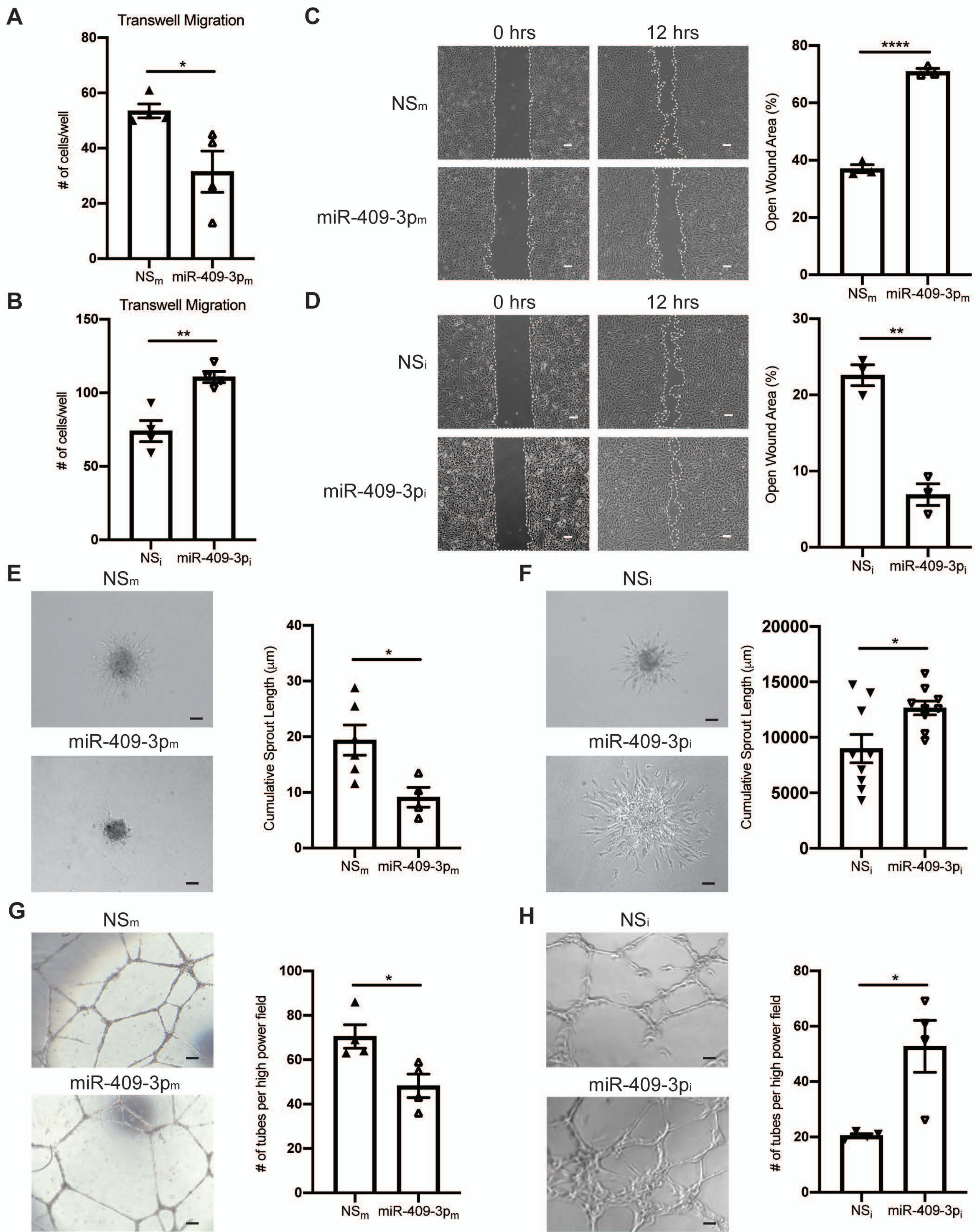

A
Transwell Migration
# of cells/well
NSm
miR-409-3pm
B
Transwell Migration
# of cells/well
NSi
miR-409-3pi
C
0 hrs
12 hrs
NSm
miR-409-3pm
Open Wound Area (%)
D
0 hrs
12 hrs
NSi
miR-409-3pi
Open Wound Area (%)
E
NSm
miR-409-3pm
Cumulative Sprout Length (μm)
F
NSi
miR-409-3pi
Cumulative Sprout Length (μm)
G
NSm
miR-409-3pm
# of tubes per high power field
H
NSi
miR-409-3pi
# of tubes per high power field

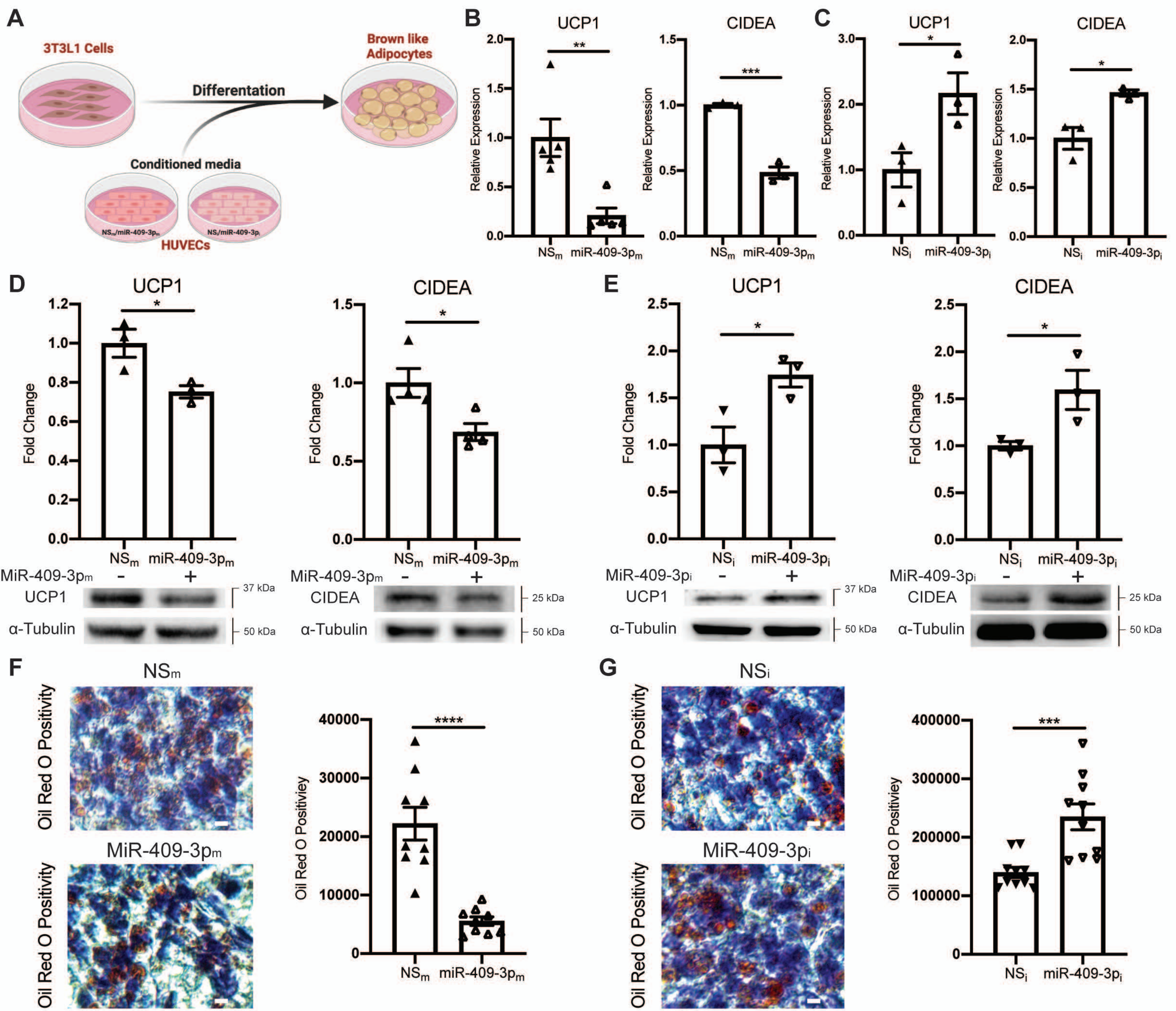
A
3T3L1 Cells
Differentation
Brown like Adipocytes
Conditioned media
HUVECs
B
UCP1
CIDEA
Relative Expression
NSm
miR-409-3pm
C
NSi
miR-409-3pi
D
E
Fold Change
MiR-409-3pm
MiR-409-3pi
α-Tubulin
37 kDa
25 kDa
50 kDa
F
G
Oil Red O Positivity
Oil Red O Positiviey
MiR-409-3pm
MiR-409-3pi

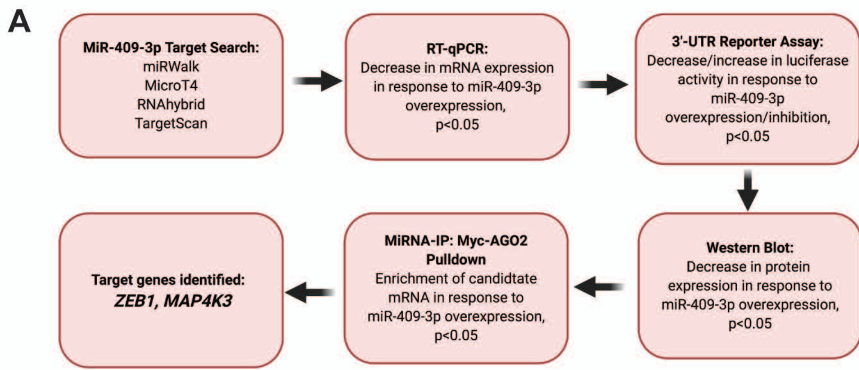
A
MiR-409-3p Target Search:
miRWalk
MicroT4
RNAhybrid
TargetScan
RT-qPCR:
Decrease in mRNA expression in response to miR-409-3p overexpression, p<0.05
3'-UTR Reporter Assay:
Decrease/increase in luciferase activity in response to miR-409-3p overexpression/inhibition, p<0.05
Western Blot:
Decrease in protein expression in response to miR-409-3p overexpression, p<0.05
MiRNA-IP: Myc-AGO2 Pulldown
Enrichment of candidtate mRNA in response to miR-409-3p overexpression, p<0.05
Target genes identified:
ZEB1, MAP4K3

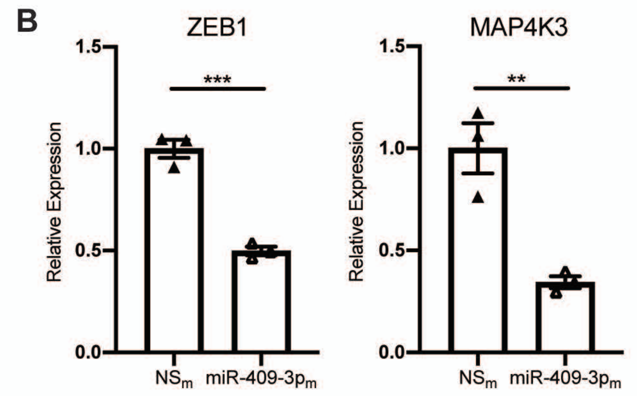
B
ZEB1
MAP4K3
Relative Expression
***
**
NSm
miR-409-3pm

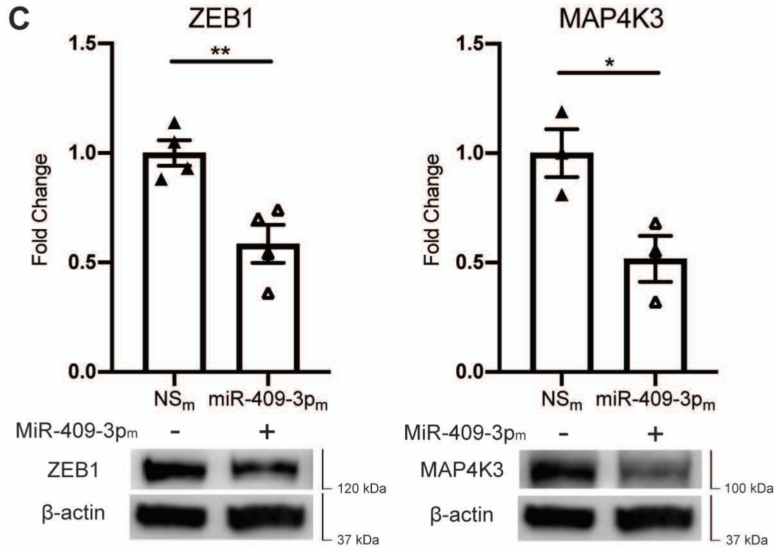
C
ZEB1
MAP4K3
Fold Change
**
*
NSm
miR-409-3pm
MiR-409-3pm
ZEB1
MAP4K3
β-actin
120 kDa
100 kDa
37 kDa

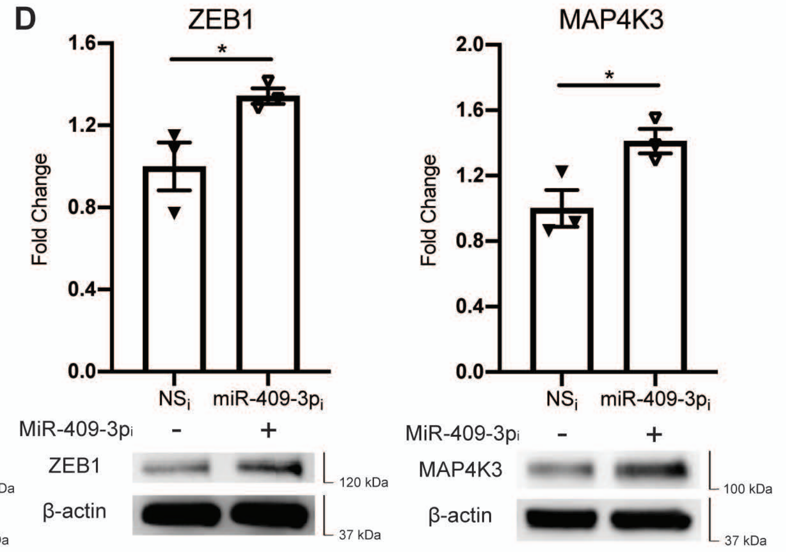
D
ZEB1
MAP4K3
Fold Change
NSi
miR-409-3pi
MiR-409-3pi
ZEB1
MAP4K3
β-actin
120 kDa
100 kDa
37 kDa

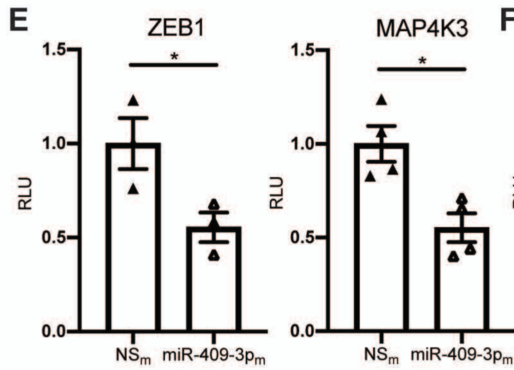
E
ZEB1
MAP4K3
RLU
NSm
miR-409-3pm

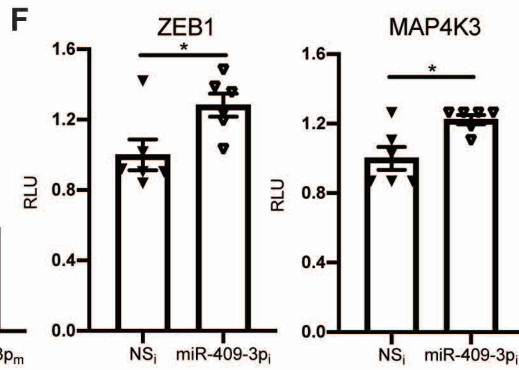
F
ZEB1
MAP4K3
RLU
NSi
miR-409-3pi

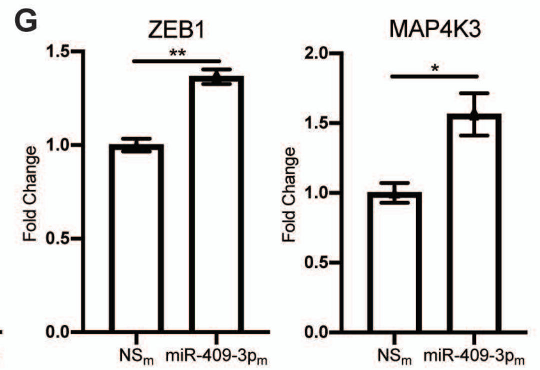
G
ZEB1
MAP4K3
Fold Change
**
NSm
miR-409-3pm

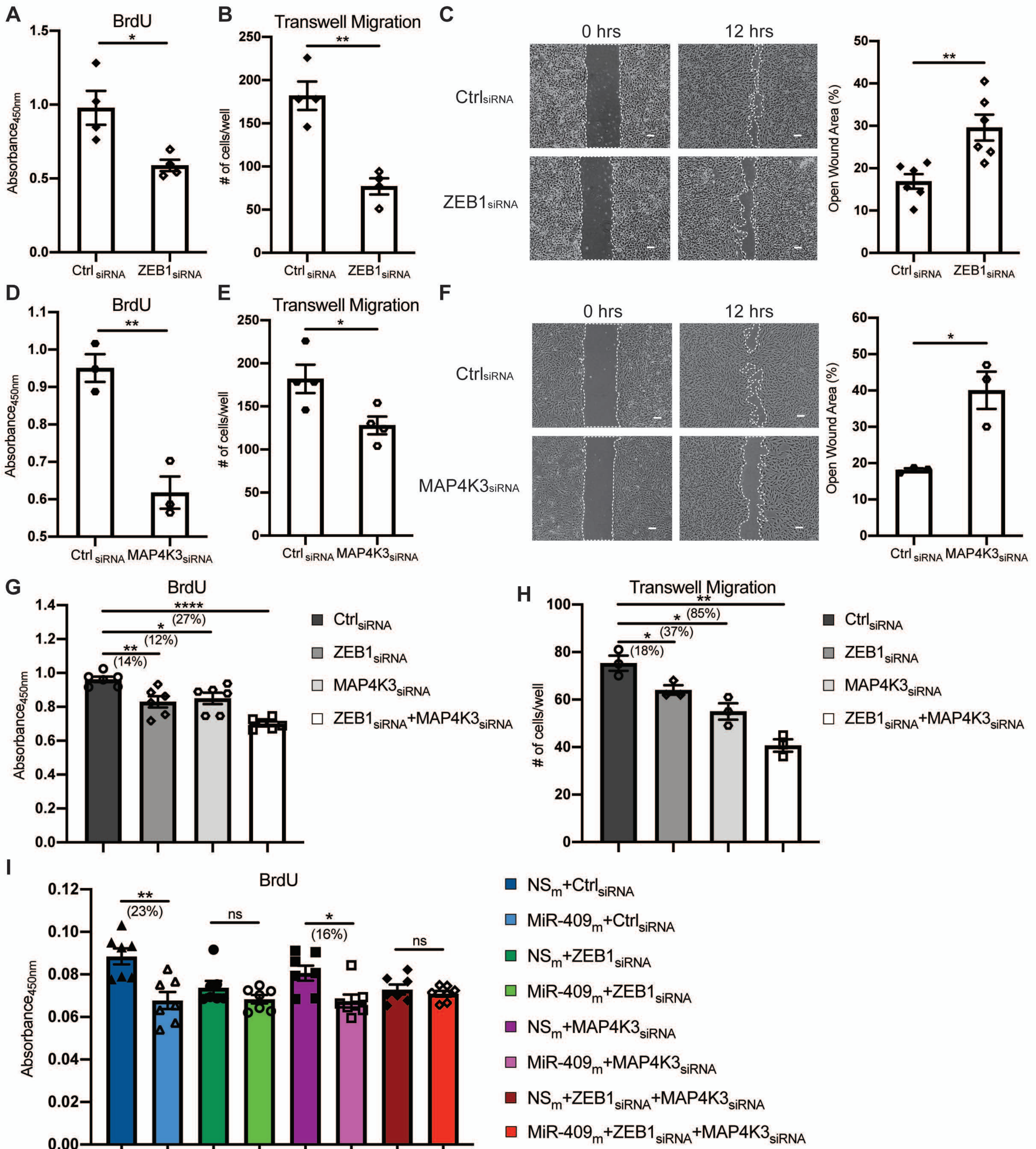

A
BrdU
Absorbance450nm
Ctrl siRNA
ZEB1siRNA
B
Transwell Migration
# of cells/well
C
0 hrs
12 hrs
CtrlsiRNA
ZEB1siRNA
Open Wound Area (%)
D
BrdU
MAP4K3siRNA
E
Transwell Migration
F
0 hrs
12 hrs
MAP4K3siRNA
G
BrdU
(27%)
(12%)
(14%)
CtrlsiRNA
ZEB1siRNA
MAP4K3siRNA
ZEB1siRNA+MAP4K3siRNA
H
Transwell Migration
(85%)
(37%)
(18%)
I
BrdU
(23%)
ns
(16%)
NSm+CtrlsiRNA
MiR-409m+CtrlsiRNA
NSm+ZEB1siRNA
MiR-409m+ZEB1siRNA
NSm+MAP4K3siRNA
MiR-409m+MAP4K3siRNA
NSm+ZEB1siRNA+MAP4K3siRNA
MiR-409m+ZEB1siRNA+MAP4K3siRNA

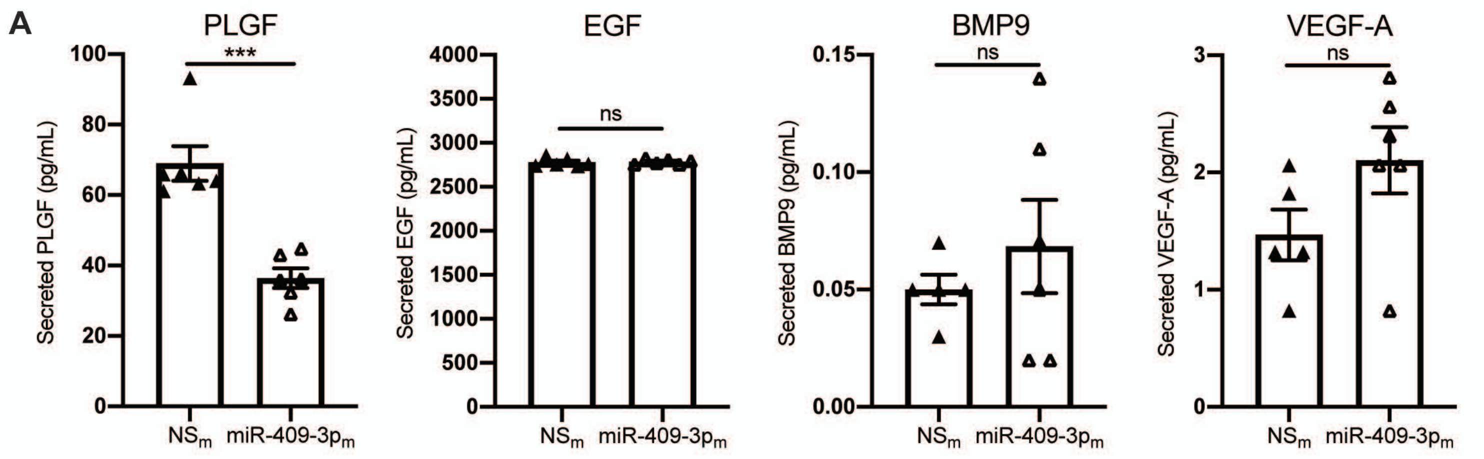
A
PLGF
EGF
BMP9
VEGF-A
***
ns
ns
ns
Secreted PLGF (pg/mL)
Secreted EGF (pg/mL)
Secreted BMP9 (pg/mL)
Secreted VEGF-A (pg/mL)
NSm
miR-409-3pm

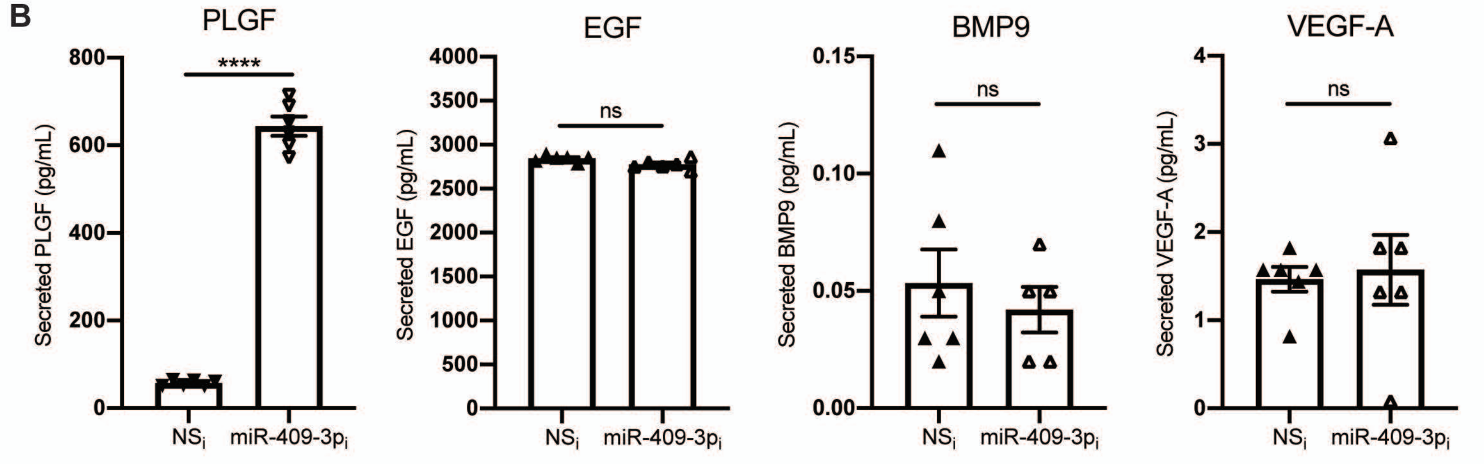
B
PLGF
EGF
BMP9
VEGF-A
****
ns
ns
ns
Secreted PLGF (pg/mL)
Secreted EGF (pg/mL)
Secreted BMP9 (pg/mL)
Secreted VEGF-A (pg/mL)
NSi
miR-409-3pi

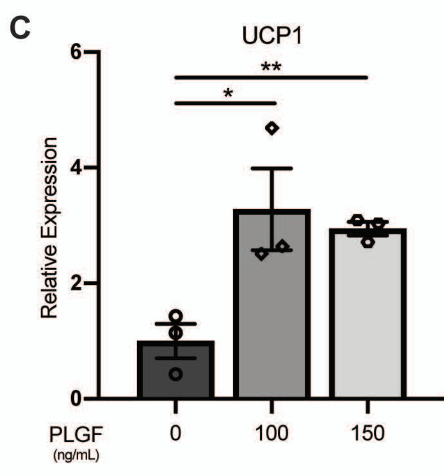
C
UCP1
Relative Expression
PLGF
(ng/mL)
0
100
150

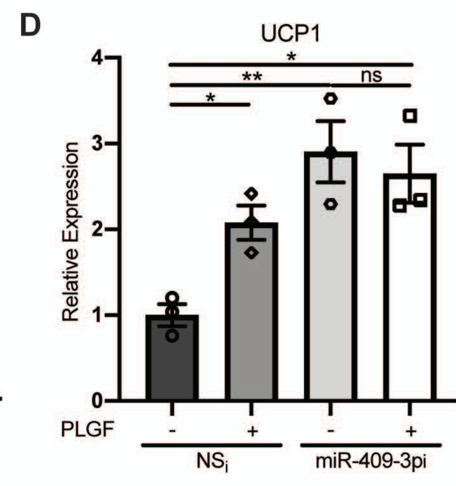
D
UCP1
Relative Expression
PLGF
NSi
miR-409-3pi
ns

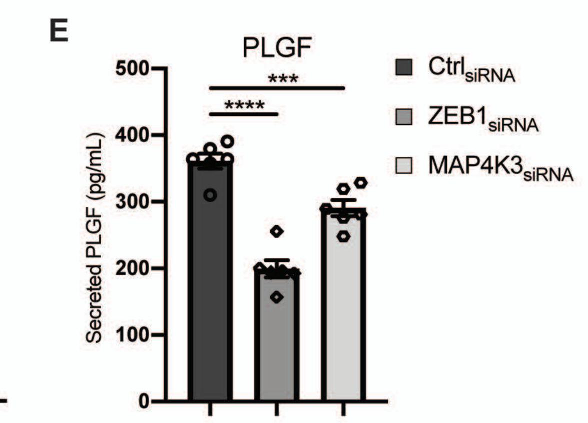
E
PLGF
Secreted PLGF (pg/mL)
****
***
CtrlsiRNA
ZEB1siRNA
MAP4K3siRNA

A

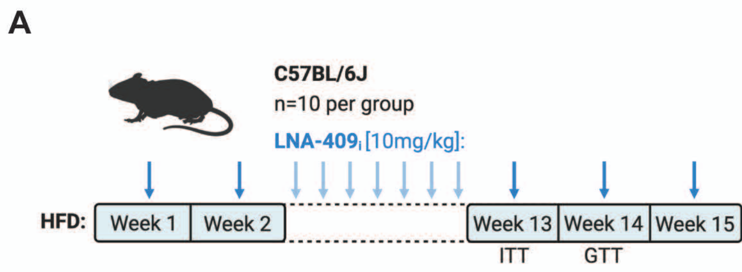

B

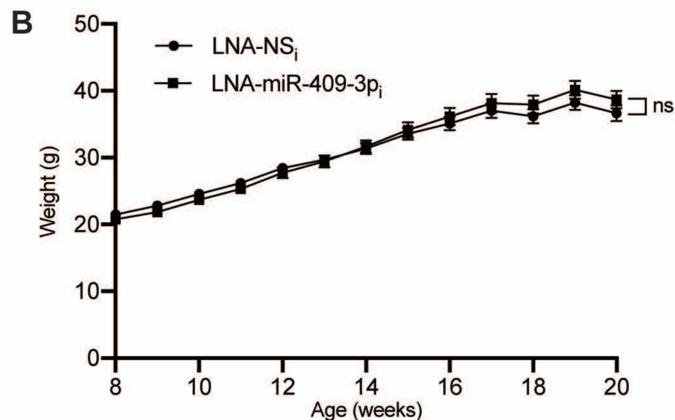

C

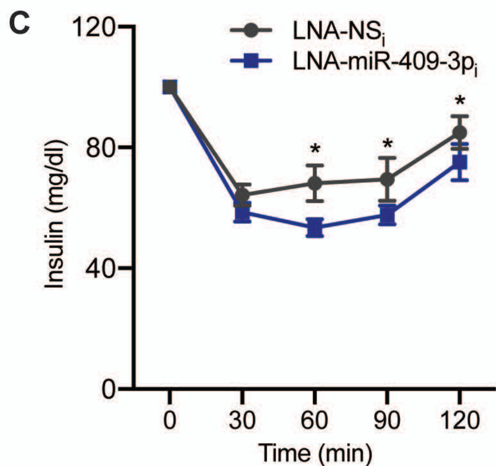

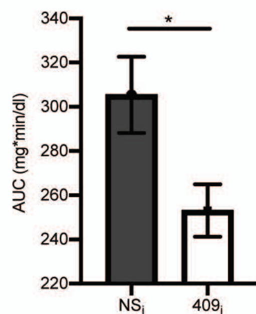

D

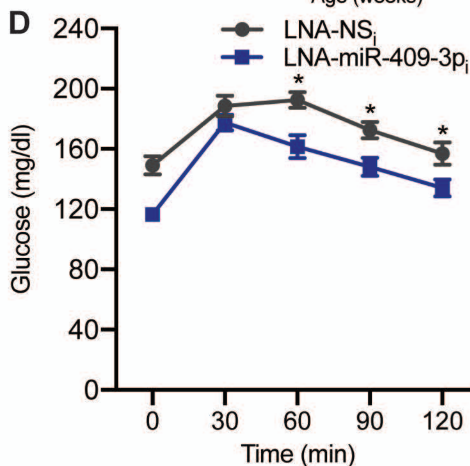

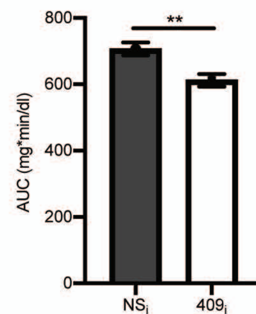

E

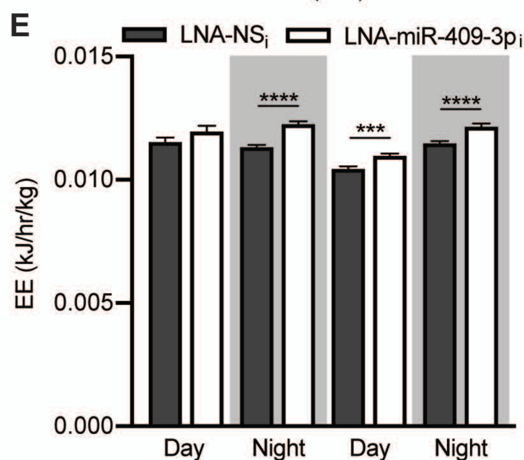

F

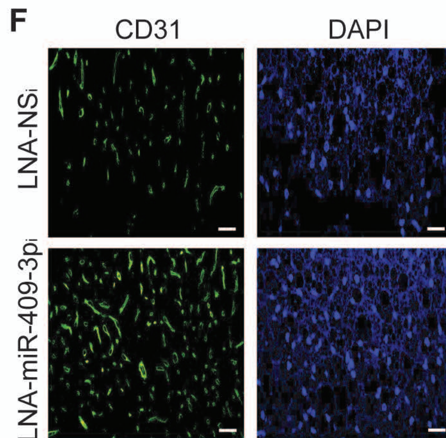

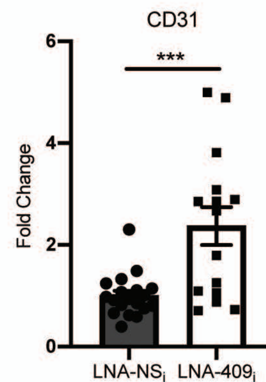

G